Measurement and Modeling of the Ability of Crack Fillers to Prevent Chloride Ingress into Mortar

Scott Z. Jones[1], Dale P. Bentz[1], Jeffrey M. Davis[2], Daniel S. Hussey[3], David L. Jacobson[3], John L. Molloy[4], John R. Sieber[4]

[1]National Institute of Standards and Technology
Materials and Structural Systems Division
100 Bureau Drive
Gaithersburg, MD 20899
E-mail: scott.jones@nist.gov, dale.bentz@nist.gov

[2]PNDetector GmbH, GERMANY
E-mail: jeff.davis@pndetector.de

[3]National Institute of Standards and Technology
Radiation Physics Division
E-mail: daniel.hussey@nist.gov, david.jacobson@nist.gov

[4]National Institute of Standards and Technology
Chemical Sciences Division
E-mail: john.molloy@nist.gov, john.sieber@nist.gov

Abstract

A common repair procedures applied to damaged concrete is to fill cracks with an organic polymer. This operation is performed to increase the service life of the concrete by removing a preferential pathway for the ingress of water, chlorides, and other deleterious species. To effectively fulfill its mission of preventing chloride ingress, the polymer must not only fully fill the macro-crack, but must also intrude the damage zone surrounding the crack perimeter. Here, the performance of two commonly employed crack fillers, one epoxy, and one methacrylate, are investigated using a combined experimental and computer modeling approach. Neutron tomography and microbeam X-ray fluorescence spectrometry (µXRF) measurements are employed on pre-cracked and chloride-exposed specimens to quantify the crack filling and chloride ingress limiting abilities, respectively, of the two polymers. A two-dimensional model of chloride transport is derived from a mass balance and solved by the finite element method. Crack images provided by µXRF are used to generate the input microstructure for the simulations. When chloride binding and a time-dependent mortar diffusivity are both included in the computer model, good agreement with the experimental results is obtained. Both crack fillers significantly reduce chloride ingress during the 21 d period of the present experiments; however, the epoxy itself contains approximately 4 % by mass chlorine. Leaching studies were performed assess the epoxy as a source of deleterious ions for initiating corrosion of the steel reinforcement in concrete structures.

Keywords: Chloride ions; crack filler; cracking; diffusion; epoxy; methacrylate; mortar; simulation.

Introduction

One of the largest components of our physical infrastructure, reinforced concrete, is often compromised by cracking and chloride-induced corrosion of steel reinforcement [1]. Mitigation strategies to reduce or eliminate cracking, especially early-age cracking, [2] have been researched and implemented, with internal curing [3] and shrinkage-reducing admixtures [4] being two prime examples. In practice, cracks continue to form, commonly within the first year following concrete placement [5]. Unfortunately, in many cases, the majority of the cracking is in the form of transverse cracks that form directly above the first layer of the steel reinforcement within the concrete. In extreme cases, the presence of these cracks can result in rapid penetration of chloride ions directly to the level of the steel reinforcement, so that corrosion can be initiated in as little as one year after completion of construction [6].

Strategies to repair concrete structures can be found in [7] and [8]. These documents provide guidance to engineers, inspectors, and owners of concrete structures so they may assess the current state of the structure and develop appropriate rehabilitation strategies. These strategies cover the use of both cementitious and polymer-based repair materials. In some cases, cracked concrete surfaces are repaired by entirely covering the surface with a sealer [9], but another common approach to remediation is to fill the cracks, especially the larger ones, with a liquid polymer that subsequently cures, or hardens, to an elastic solid, and is intended to prevent subsequent ingress of water, chlorides, and other deleterious species into the concrete at the crack site. The focus of the current study is limited to organic polymers, specifically epoxies and methacrylates. Few guidelines exist on the selection and performance evaluation of these materials for concrete applications, although some guidance can be found for filling cracks in asphalt surfaces [10]. At a minimum, these materials must possess an appropriate viscosity to flow into and completely fill the crack, a reasonable curing time under expected field conditions, and physical properties in the hardened state (e.g., elastic modulus, strain capacity, and coefficient of thermal expansion) that enable them to remain in place and prevent the ingress of water and deleterious species such as chloride ions. Another natural consideration should be the chloride content of these polymers and whether any chloride they may contain is permanently bound or mobile.

This paper presents an evaluation of the performance of two crack fillers in preventing the ingress of chloride ions, via diffusion, into cracked mortar specimens. A combination of experimental and computer modeling techniques [11-16] are employed to evaluate their efficacy in reducing chloride penetration. Neutron tomography is employed to estimate the penetration of the crack filler into the surrounding mortar and the results are used to guide the selection of the damage zone diffusivity for the case of a repaired crack.

Materials and Methods

Cracked Mortar Beams

Simply reinforced mortar beams, measuring 4 cm x 4 cm x 16 cm, were created using a mixture of ASTM C150 Type I portland cement [17], water, and a blend of four silica-containing sand. Mixture proportions are reported in Table 1. The cement was a Cement and Concrete Reference Laboratory (CCRL) proficiency cement number 192 (issued in January 2014). Chemical analyses were obtained from the consensus values available from CCRL (www.ccrl.us). Two

water-to-cement ratios by mass were studied, $w/c = 0.4$ and 0.5. These w/c values produce mortars with different effective diffusivities. All materials were weighed to the nearest 0.1 g. A blend of 4 sands were used to prepare the mortar: two ASTM C778 sands and two commercially available silica sands listed as "Coarse" and "Fine" in Table 1. The coarse sand had a maximum size of 2 mm while the fine sand had a median particle diameter of 0.13 mm ± 0.02 mm [18].

Table 1. Mixture proportions in grams of material per batch

	$w/c = 0.4$	$w/c = 0.5$
Cement	637.1	637.1
Water	254.8	318.6
Fine sand	357.1	357.1
ASTM C778 [17] graded sand	271.4	271.4
ASTM C778 20-30 sand	271.4	271.4
Coarse sand	528.5	528.5

A single 16 cm length of threaded stainless steel rod was placed at the center of the beams and served as reinforcement. All specimens were cured a 23 °C to 7 d sealed in a plastic bag containing approximately 10 mL of water to maintain a 100 % RH environment. After 7 d, a portion of the beam specimens were cracked, at their mid-span point, in three-point bending by cutting a 2 mm wide by 4 mm deep pre-crack notch into the finished surface. A monotonically increasing load was applied to the beam at its mid-span. The magnitude of the applied force was monitored and recorded by the control system of the universal testing machine (UTM). The load was applied until a peak load was observed, typically between 3 kN and 4 kN. The test was stopped before the mid-span displacement, as indicated by cross-head position, reached 1.5 mm. All specimens were sealed with paraffin wax on all sides except for the finished surface; i.e., the notched surface. Cracked specimens were repaired with either an epoxy or a methacrylate crack filler or remained in their cracked state without repair. The crack fillers used in this study are two-component systems and were prepared according to manufacturer specifications. Crack repairs were made by filling the pre-crack notch with the crack filler, using a syringe. The combination of the gravitational force and capillary action drew the crack-filling material into the crack from the pre-crack notch. As the crack filler penetrated the crack, additional material was added to the pre-crack notch until it began to overflow to the surrounding area. The specimens were kept in laboratory atmospheric conditions for 24 h to allow the crack filler to cure. After the crack filler cured, the specimens were returned to sealed curing conditions. When the specimens reached an age of 28 d, all specimens (uncracked, cracked, and crack-filled) were placed in a 1000 mol/m^3 NaCl solution maintained at 23 °C, until being removed for μXRF analysis. Specimens were exposed to the NaCl solution for 7 d to 21 d. After removal from the chloride solution, specimens were placed in a freezer at -10 °C, at atmospheric pressure, to slow subsequent diffusion. Samples were prepared for μXRF analysis by sectioning the beams into thirds and cutting perpendicular to the crack with a diamond saw. Cuts were made in 200-proof ethanol to limit disruption of bound chloride ions in the hardened cement paste. The surfaces to be scanned were polished with 120 grit SiC abrasive paper and ethanol.

Crack Fillers

Two commercially available crack fillers were investigated in this study, an epoxy and a methyl methacrylate (MMA). Exact chemical formulations are proprietary, but the Safety Data Sheet (SDS) indicates that the epoxy's primary component is 4,4'-(2-2-Propanediyl)diphenol-2-(chloromethyl)oxirane (linear formula: $C_{15}H_{16}O_2 \cdot C_3H_5ClO$), and the methacrylate's primary component is an aliphatic methacrylate ester. Table 2 reports several properties of the crack fillers published in their manufacturers' product documentation.

The chemical composition of the crack fillers was estimated by Wavelength Dispersive X-ray Fluorescence (WDXRF) of a cured specimen. The results are reported in [16] and show the epoxy crack filler contains approximately 4 % Cl, by mass.

Table 2. Properties of epoxy and methacrylate crack fillers as reported in manufacturers' product documentation

Property (Test Procedure)	Epoxy[1]	Methacrylate[2]
Viscosity	0.375 Pa-s	0.025 Pa-s
7 d Tensile Strength (ASTM D-638)	61.4 MPa	--
14 d Elastic Modulus (ASTM D-638)	2800 MPa	--
7 d Elongation at Break	5.4 %	--
7 d Water Absorption (ASTM D-570)	0.27 %	--
7 d Compressive Strength (ASTM D-695)	75.9 MPa @ 23 °C 72.5 MPa @ 32 °C	24.1 MPa @ 4 °C 21.3 MPa @ 23 °C 29.6 MPa @ 32 °C
7 d Compressive Modulus	1863 MPa	--
1 d Flexural Strength (ASTM D-790)	96.6 MPa (14 d)	17.2 MPa (1 d)
14 d Bond Strength (ASTM C-882)	20.0 MPa	15.8 MPa

[1] Product data sheet dated 07-23-2014
[2] Product data sheet dated 05-04-2011

Mortar Characterization – Binding and Time-Dependent Diffusivities

Transport of chloride ions into the mortar depends on its chloride-binding capacity and time-dependent diffusivity. Chloride binding isotherms were determined by allowing pulverized mortar to reach adsorption equilibrium as described in [19]. Pulverized mortar was passed through a 1680 µm sieve and divided into 30 g samples and each sample was submerged in an aqueous NaCl, with a concentration between 10 mol/m^3 to 1500 mol/m^3, until adsorption equilibrium was achieved. The concentration of the solution containing the pulverized mortar was measured using a chloride selective electrode and the difference between the initial NaCl concentration and the

equilibrium NaCl concertation is assumed to be the total chloride concentration bound to the mortar.

To determine the time-dependent diffusivity of the mortar, the resistivity of the pore solution is determined as a function of mortar age. Pore solution is extracted by the procedure described in [16], and the resistivity is measured by the procedure described in [14-16]. Bulk mortar resistivity was determined by measuring the resistance of the mortar contained in a 76 mm diameter by 152 mm long cylindrical container. Calibration of this cell was achieved by measuring the resistance of solutions of known resistivity, as described in [14-16,20]. The Nernst-Einstein equation, Equation 1, was used to estimate the diffusivity from the pore solution and mortar resistivities, which relates the resistivity of the pore solution and mortar to the diffusivity of the ions contained in the mortar's pore solution.

$$\rho_c/\rho_{ps} = D_0/D(t) \tag{1}$$

In Equation 1, ρ_c is the mortar resistivitiy, ρ_{ps} is the resistivity of the pore solution, D_0, is the chloride ion self-diffusivity in water, and D(t) is the effective diffusivity of chloride ions through the water-filled pore structure of the mortar. To facilitate implementing the experimental measurements in a numerical model, non-linear regression of the resistivity measurements was used to fit the pore solution resistivity and mortar diffusivity to Equations 2 and 3, respectively.

$$\rho_{ps} = C + A \cdot t^b \tag{2}$$

$$D(t) = D_\infty + D_i \cdot t^m + D_{ib} \cdot t^l \tag{3}$$

The functional form of Equations 2 and 3 were based on observations and chosen to produce the best fit of the experimental data. Regression of the measurements with Equation 3 produced an exponential value greater than 1 for the parameter m. This value should be less than 1 for valid analytical solutions to Fick's Law, but in numerical approximations, values greater than 1 can be employed [21]. The diffusivity of the domain bounded by the crack is assumed to be D_0, when the crack is saturated with a chloride containing solution, and the epoxy or methacrylate diffusivity is estimated by the procedure outlined in [13,16]. The effect of the crack filler on water absorption resulting from capillary action is not considered in this study. The functional form shown in Equation 4 was used to represent the chloride binding isotherm for the mortars where C_{free} is the concentration of chloride ions in the pore solution and $C_{bound-eqbm}$ is the equilibrium concentration of chloride ions that have become bound to the solid phases by chemical or physical adsorption.

$$C_{bound-eqbm} = \frac{\alpha C_{free}}{1 + \beta C_{free}} \tag{4}$$
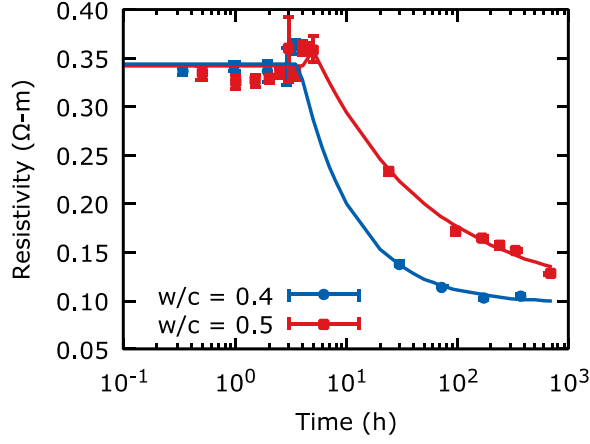
The parameters produced by non-linear regression of Equations 2 through 4 are reported in Tables 3 and 4, and the plots of experimental measurements with regression curves are given in Figure 1. The model assumes no chlorides are bound in the domain comprised of the crack (filled or unfilled).

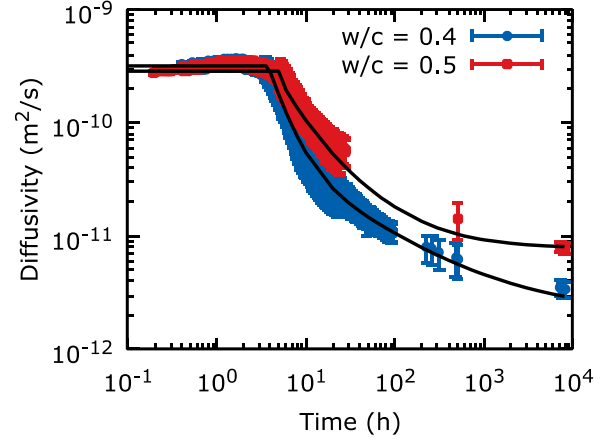**Table 3.** Curve fit parameters for pore solution resistivity and diffusivity of mortars.

Parameter		Value	Std. Error		Value	Std. Error
w/c = 0.4	C	0.0972 Ω-m	0.0034 Ω-m	D_∞	2.143E-12 m^2/s	1.92E-13 m^2/s
				D_i	6.910E-09 m^2/s^2	2.09E-10 m^2/s^2
	A	0.7805 Ω-m/s	0.0501 Ω-m/s	D_{ib}	9.932E-11 m^2/s^2	3.52E-12 m^2/s^2
				m	-2.467E+00	2.1E-02
	b	-0.8782	0.0589	l	-5.37E-01	1.2E-02
w/c = 0.5	C	0.1027 Ω-m	0.0143	D_∞	7.821E-12 m^2/s	4.20E-13 m^2/s
				D_i	3.487E-09 m^2/s^2	2.54E-10 m^2/s^2
	A	0.5022 Ω-m/s	0.0286	D_{ib}	4.868E-10 m^2/s^2	6.95E-11 m^2/s^2
				m	-2.113E+00	9.7E-02
	b	-0.4193	0.0575	l	-8.424E-01	3.8E-02

Table 4. Parameters determined from non-linear least squares regression of Langmuir isotherms of chloride binding measurements.
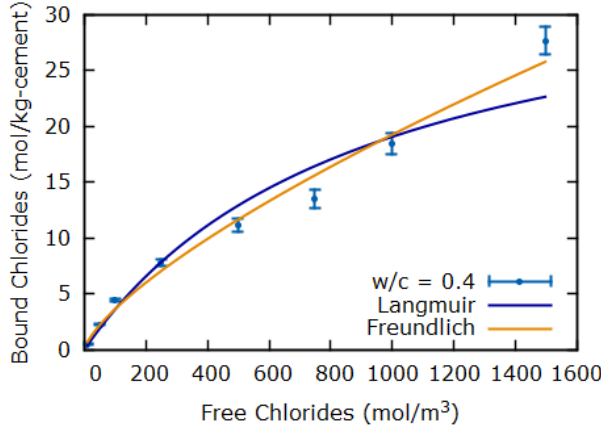
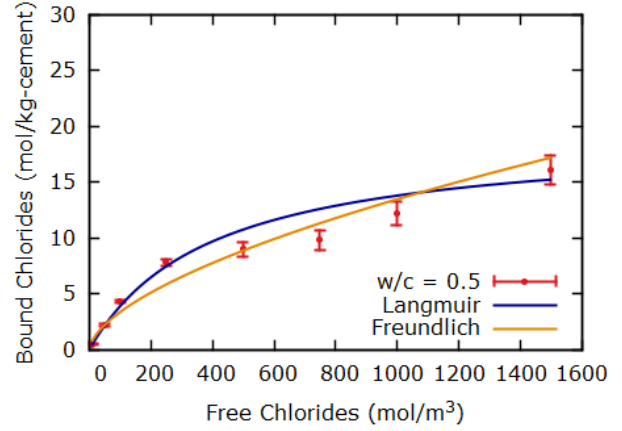| Isotherm		*w/c* = 0.4		*w/c* = 0.5	
		Value	Std. Error	Value	Std. Error
Langmuir	α	4.01E-02	6.4E-03	4.890E-02	2.2E-04
	β	1.10E-03	4.0E-04	2.54E-03	3.6E-04

(a) Pore Solution Resistivity

(b) Mortar Diffusivity

(c) Cl⁻ Binding, *w/c* = 0.4

(d) Cl⁻ Binding, *w/c* = 0.5

Figure 1. Mortar transport properties: (a) pore solution resistivity, (b) mortar diffusivity, and Cl⁻ binding for (c) *w/c* = 0 .4 and (d) *w/c* = 0.5

   Transport of chloride ions through the cement paste is derived from a mass balance on an infinitesimal volume of the domain of interest [16]. Formulating the governing equations in the paste is equivalent to assuming that the aggregates do not absorb or transport chloride ions. Within the paste, chloride transport is assumed to occur through the water saturated pore structure. The flux across a face of the control volume is $j = D(t)\nabla C_{f-pore} = \epsilon_p D(t) C_f$ where C_{f-pore} is expressed in terms of water accessible pore volume, C_f is expressed in terms of paste volume and ϵ_p is the water accessible porosity of the paste. The time rate of change of the chloride concentration in the paste volume is equal to the sum of the flux going into the volume minus the flux leaving the volume plus accumulations of chlorides inside the volume. This is expressed mathematically in Equation 5 where Fick's Law is used to relate the flux to the free chloride concentration (C_f). In Equation 5, the binding of free chlorides to the mortar matrix is modeled as a first order reaction with reaction rate k. The change in concentration of bound chlorides (C_{bound}) is described by Equation 6, which combines the absorption of the chlorides by calcium silicate hydrate gel (C-S-H) and formation of Friedel's salts and other chloride-bearing compounds.

$$\frac{\partial C_f}{\partial t} = \nabla \cdot \left(\epsilon_p D(t) \nabla C_f\right) + k\left(C_{bound} - C_{bound-eqbm}\right) \tag{5}$$

$$\frac{dC_{bound}}{dt} = k\left(C_{bound-eqbm} - C_{bound}\right) \tag{6}$$

µXRF Measurements

Chloride concentrations were determined from chlorine measurements made using an EDAX Eagle III microbeam X-ray fluorescence spectrometer with a Rh X-ray source and a 25 µm thick Al primary beam filter[1]. The X-ray tube voltage and current were set to 40 kV and 1000 µA, respectively. The nominal beam spot size was 50 µm, and the area measured was approximately 14 mm by 20 mm, centered on the crack. To ensure the X-ray beam covers the entire area of interest, measurements were made at 25 µm intervals corresponding to approximately half X-ray beam overlap. The specimen was placed on a translating stage and moved in a raster pattern under the stationary X-ray beam. Spectra were acquired for 400 ms per location with the detector pulse shaping time set to 12.8 µs. X-Ray counts for Cl and other elements in the cement matrix were obtained from each spectrum by fitting peaks, after escape peak removal and background subtraction was performed in EDAX Vision 32, version 4.992-977R software[1].

Calibration of µXRF data was achieved by preparing mortar specimens, composed of the same materials as the test specimens and in the same proportions, with known additions of chloride ions. The data output from the µXRF is in the form of a spectrum of counts vs. electron volts (eV) at each pixel. For each standard, the counts in the range of 2.40 keV to 3.00 keV (corresponding to Cl Kα and Cl Kβ lines) at each pixel were fit to a gamma distribution [16]. A linear model was assumed ($Y = \beta_1 X$), and the added chloride concentration was regressed onto the expected values of the counts. Table 5 reports the estimated β_1 value for a mortar with *w/c* = 0.4 and 0.5.

Table 5. Coefficient estimates of linear $Y = \beta_1 X$.

w/c		Est. (mol/m^{3}count)	Std. Error (mol/m^{3}count)	*t*-statistic	*p*-value	DoF
0.4	β_1	0.0378	2.4E-03	15.74	2.66E-07	8
0.5	β_1	0.0356	2.3E-03	15.74	2.66E-07	8

Support Vector Machine and Generalized Additive Model

The data of interest is the chloride ion concentration in the cement paste. Pixels from the coarse and fine aggregates and epoxy, as well as the interfacial transition zone around the aggregates, were not included in the concentration model. Since cement paste contains Si, Ca, and varying amounts of Cl, simple linear combination models are not sufficient to adequately segment the elemental data. Further, the case of an analysis point that contains both cement and aggregate needed to be addressed. A training data set was collected from a mortar sample, of the same mix design, and was scanned under the same scan settings as the test specimens. All samples in this study were made with CCRL 192 cement, which contains 0.031 % Cl, by mass. The training data

---

[1] Certain commercial products are identified in this paper to specify the materials used and the procedures employed. In no case does such identification imply endorsement or recommendation by the National Institute of Standards and Technology, nor does it indicate that the products are necessarily the best available for the purpose.

set was used to train a support vector machine (SVM) to distinguish between the aggregate and paste phases. The SVM does not rely on a linear combination of elemental compositions or on a defined count range. Rather, the model can separate out the data purely from the resulting X-ray spectrum, and, as a result, it is very efficient for processing the data and extracting the phase information. Only the X-ray counts in the paste phase are of interest to this study as the transport of chloride ions occurs through the saturated and percolated pore structure of the cement paste. A generalized additive model (GAM) was used to interpolate between the chloride counts over the scanned domain. A square root link function was used, and the number of knots required for the smoothing splines was determined by three-fold cross validation. Complete details of the use of SVM and GAM for this study are given in [16] while the derivation of these statistical analyses are given in [22-24].
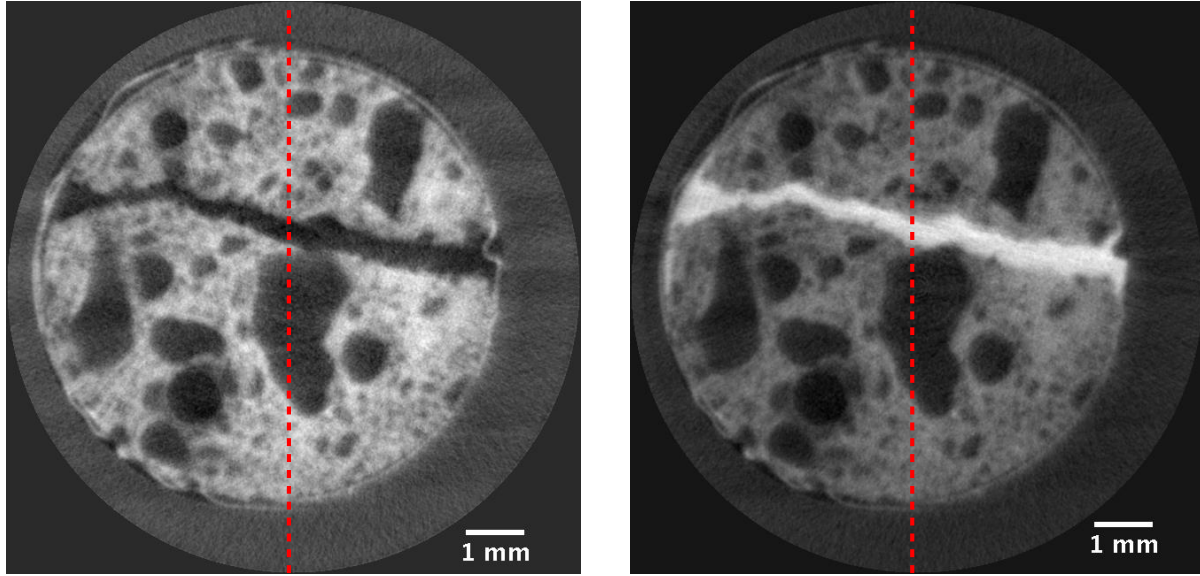
Neutron Tomography Sample Preparation

Neutron tomography of a crack before and after crack filling is used to estimate the depth of penetration of the crack filler into the mortar. Slightly larger beams, 5 cm x 5 cm x 15 cm, of mortar were prepared. The beams were placed into a plastic bag and kept at a 23 °C for 7 d, at which time they were subjected to a three-point bending load to generate a crack. After cracking, the average crack mouth opening was measured to be 351 μm (standard deviation of 25 μm on 10 replicate measurements) for the crack to be filled with epoxy and 242 μm (standard deviation of 16 μm on 10 replicate measurements) for the methacrylate-filled crack. After 14 d subsequent curing, a 6 mm diameter coring bit was used to core the empty crack. The cored crack was stabilized with refractory clay and placed into a PTFE sample holder. The empty crack sample was placed onto a rotation stage within the neutron beam at the NIST neutron imaging facility. After the empty crack scan, each crack was gravity filled by dispensing about 5 mL of the crack filler on top of the crack opening. The crack filler cured for 1 h before the start of the filled crack scan

Both the empty crack and filled crack scan were completed with a fluence rate of 1.37×10^7 cm^{-2}s^{-1} and collimation ratio of 450 [25]. A gadolinium oxysulfide scintillator converts the neutrons to a light signal that is captured by a complementary metal oxide semiconductor camera, with an effective pixel pitch of 15 μm. Each specimen was rotated 180° in increments of 0.25°, with five images (20 s exposure) taken at each angle. The five images are averaged together and a three-dimensional tomographic reconstruction is performed using the filtered back projection algorithm.

Crack Filler Penetration Depth

After reconstruction, the tomography data consist of a set of 32-bit gray scale images of the sample's cross-section, corresponding to 15 μm thick slices. Two representative images are shown in Figure 2. Crack filler penetration depth is estimated from the slices by plotting the gray scale value (GSV) along the red dashed line, shown in Figure 2, and subtracting the widths of the peaks corresponding to the empty and filled cracks. The GSVs of the empty and filled cracks for one slice is shown in Figure 3, which identifies the peak or valley corresponding to the filled or empty crack. Analysis of the tomography slices is performed in the statistical computing package R [26]. The GAM is fit to the data using the mgcv package and the peak width is estimated with the pracma package [27,28]. The function findpeaks is contained within the pracma package

and is used to estimate the peak width. The function returns the values within the domain corresponding to the peak beginning and end. The peak width is taken to be the difference between these values. The change in peak width from the empty to filled crack corresponds to the total penetration of the crack filler into the mortar [16].

(a) Empty Crack   (b) Epoxy-Filled Crack

Figure 2. Reconstructed image of an epoxy filled crack (a) before crack filling and (b) after crack filling. The GSV is plotted along a line approximately perpendicular to the crack in the center of each image.

Figure 3. GSVs along the red dashed lines in Figure 2. Crack filler penetration is estimated by subtracting the empty crack peak width from the filled crack peak width.

Computer Modeling

Total chloride concentration within the mortar is estimated by solving Equations 5 and 6 by the finite element (FE) method using the commercial software package COMSOL Multiphysics, version 5.1[1]. Mesh refinement and error estimation of the FE solution is given in [16]. The control case considered in this study is a mortar without a crack. The geometry of the control case is given in Figure 4a. Two domains are utilized; a domain representing the NaCl solution in which the mortar beams were stored and a domain representing the mortar. In the FE software, the transport properties of each domain are supplied as inputs in accordance with Equations 1 through 6.

FE simulations of cracked mortar are performed as in the control case, but with a few important modifications to the model. The crack geometry is imported to the FE software by combining the Si and Ca μXRF images, converting them to a binary image, and then adjusting the threshold such that only the crack outline is visible [16]. Previous studies attempting to simulate chloride concentration around cracks have assumed a region around the crack has diffusivity properties different from the bulk. Jones et al., 2015 [13] and Bentz et al., 2013 [12] assumed this region to be approximately 4 mm from the crack face, based on experimental evidence reported in [29]. In Figure 4b the damage zone region is defined by the red rectangle and was rotated around its center point to account for the tortuous crack path. The flux through the damaged zones is derived assuming the principal directions of chloride transport are aligned with the x and y axes. To account for the rotation of the damaged zone, a rotation is applied to the diffusivity tensor which produces components $D_{xx} = D_{yy} = DF \cdot D(t) \cos(\theta)$ and $D_{xy} = D_{yx} = -DF \cdot D(t) \sin(\theta)$ where DF is a parameter used to estimate the local increase in diffusivity [16]. For all simulations and experimental methods, the mortar was exposed to a $1000\ mol/m^3$ NaCl solution.

To assess agreement between the mass balance model of chloride ion transport and experimental measurements of chlorine concentration, the FE solution to Equations 5 and 6 is plotted with µXRF measurements along three parallel lines located at x = (1/4)W, (1/2)W. and (3/4)W, where "W" is the maximum x-axis value (see Figure 4a). When the specimen contains a crack, the domain of the FE simulation and scanned with µXRF is positioned such that x = (1/2)W is approximately centered along the length of the crack.

(a) Control Geometry   (b) Cracked Geometry

Figure 4. (a) Control and (b) cracked mortar geometry. FE simulations are compared to µXRF measurements by plotting the corresponding results along the three parallel lines with respect to the x-y coordinate system shown in (a). For the cracked case (b), the domain is divided up into regions representing the mortar, chloride solution, crack filler, overflow region, and the damage zone. The coordinate rotation is applied in the damage zone to align the region with the crack path.

Results and Discussion

Un-cracked Mortar

The control case was assumed to be a mortar without a crack. This scenario is considered the "best case" for the protection of the rebar from corrosion and serves as a reference for the ability of the model to predict chloride ion concentration. Figures 5 and 6 report the chlorine concentration measured by µXRF and the FE solution to the mass balance model described in [16] for mortar exposed to a 1000 mol/m^3 NaCl solution with a *w/c* = 0.4 and 0.5. Figures 5b and 5d, as well as 6b and 6d, compare chlorine measurements to FE simulation results. At each x-location, the chlorine measurements are plotted with dots and the shaded region represents the measurement uncertainty at a 95 % confidence interval (CI) determined by the procedure described in [30]. The solid and dashed lines in Figures 5b and 5d are the chloride concentrations predicted by the FE simulation at x-locations corresponding to the chlorine measurements.
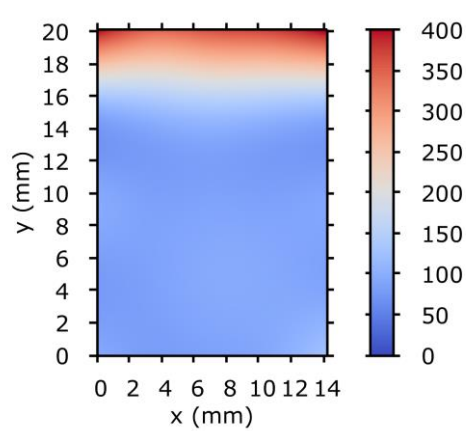
Figures 5a-b and Figures 5c-d show FE simulation and chlorine measurement results for mortar exposed to a NaCl solution for 7 d and 15 d, respectively. Figure 5 shows good agreement between the FE simulations and chlorine concentration measurements. In Figure 5b, the model is within the measurement uncertainty. Figures 6a-d report the results for the control case with

w/c = 0.5. The chloride ion transport model (Equations 5 and 6) agrees well with the chlorine concentration measurements near the top surface in Figure 5b, but underestimates the measured values as the distance increases. This may be a result of the calibration procedure, as the assumption that the calibration curve has a zero intercept, see Table 5, may be too restrictive. However, the model does follow the global trend of the chlorine concentration measurements.
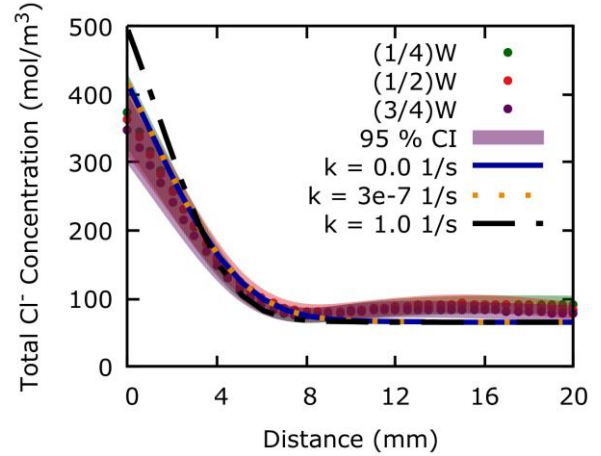
In previous modeling studies, the chloride binding reaction rate was assumed to be $3.0E-07 \ s^{-1}$ [12, 13]. In this study, the chloride binding reaction rate can be estimated by taking the inverse of the time to achieve an equilibrium concentration in the chloride binding experiments. Equilibrium was achieved in approximately 2 d, which corresponds to a reaction rate of $k = 5.7E-06 \ s^{-1}$. Since the time to the equilibrium of the chloride binding experiments is dependent upon the particle size of the pulverized mortar, i.e., smaller particle size mortar will have more surface area per unit mass, it is likely that the effective reaction rate would be slower in a system where chlorides are diffusing through a pore structure, as the surface area available for chloride binding, would be much lower.

To study the influence of k on the FE simulation results, simulations were run with $k = 1.0 \ s^{-1}$, $3.0E-07 \ s^{-1}$, and $0 \ s^{-1}$. Figures 5b and 5d (and Figure 6b and 6d) report the influence of k on the simulation results and indicate that the model is not sensitive to the reaction rate so long as the time steps taken by the solver are long enough to allow for the binding reaction to reach equilibrium. Chlorine measurements suggest chloride binding is happening at a rate closer to the assumed value of $3E-07 \ s^{-1}$. When the reaction rate is reduced, the influence of chloride binding is diminished, as a k approaching 0 removes the chloride binding term from the mass balance and the transport of chlorides is not dependent on the interaction between the chloride ions and the matrix. A binding reaction rate of zero implies an infinitely long time is required for the reaction between the matrix and chloride ions to reach equilibrium. The insensitivity of the model to the reaction rate, k, may indicate that this parameter may not play a dominant role in the resulting chloride concentration and that the transport of chlorides is more sensitive to other model parameters such as the diffusivity and chloride-loading boundary conditions. Still, the simulation results are within the measurement uncertainty, indicating that the simulation may provide a suitable estimation of chloride concentration at a given position and time.
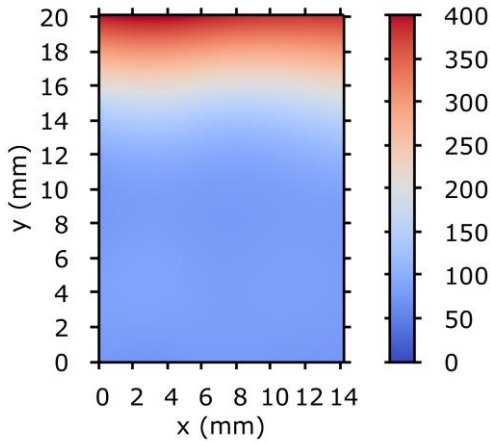
Deviation of the measured chlorine concentration from the FE simulation results may be explained by increased porosity due to leaching of portlandite and decalcification of C-S-H resulting from hydrolysis of the cement paste [31] or due to aggregate segregation resulting in variations in the paste volume fraction. The latter scenario is described in [16] where the volume fraction of the paste is estimated from μXRF measurements. This change will affect the X-ray counts due to decreases in grain size resulting from the increased porosity due to segregation of the large sand particles [32].
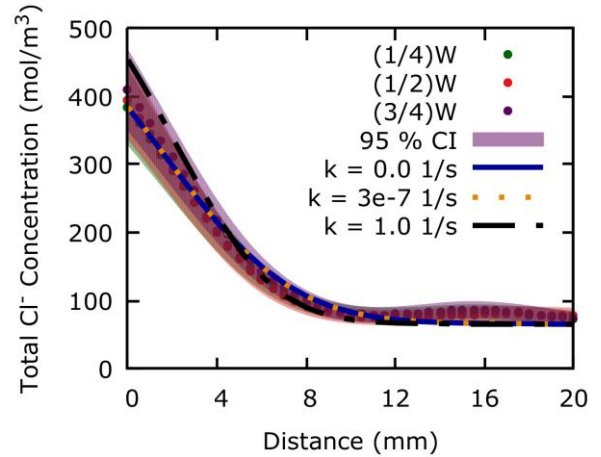
(a) µXRF Results – 7 d

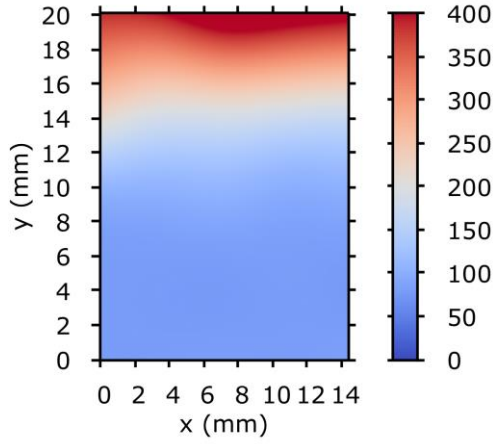(b) FE Simulation Results & µXRF
Measurements with Uncertainty

(c) µXRF Results – 15 d
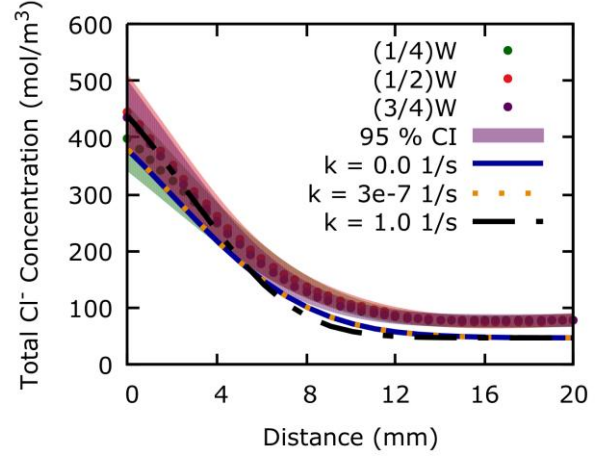

(d) FE Simulation Results & µXRF
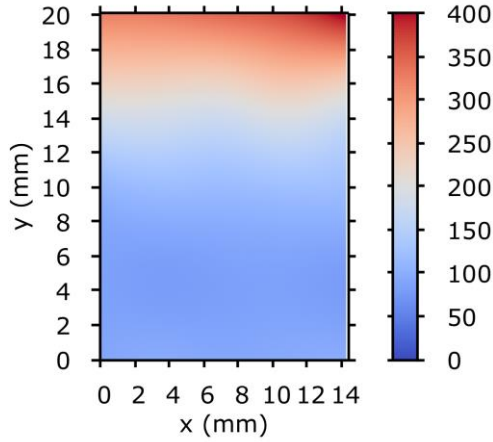Measurements with Uncertainty

Figure 5. Chlorine concentration in control specimen with w/c = 0.4 and exposed to 1000 mol/m^3 solution. Figures 5a & 5b report the results at 7 d and Figures 5c and 5d report the results at 15 d. Figures 5a & 5c report Cl concentration measured by µXRF. Figures 5b & 5d report the Cl$^-$ concentration, predicted by the FE simulation described in [16], and the Cl concentration in Figures 5a & 5c along x = (1/4)W, (1/2)W. and (3/4)W. In Figures 5b & 5d, Cl concentration measurements, by µXRF, are plotted with dots and the shaded region indicates the measurement uncertainty estimated at a 95 % confidence level. FE simulation results are plotted with dashed or solid lines. Concentration is expressed in mol/m^3 of mortar.

(a) μXRF Results – 11 d

(b) FE Simulation Results & μXRF
Measurements with Uncertainty

(c) μXRF Results – 21 d

(d) FE Simulation Results & μXRF
Measurements with Uncertainty

Figure 6. Chlorine concentration in control specimen with w/c = 0.5 and exposed to 1000 mol/m^3 solution. Figures 6a & 6b report the results at 11 d and Figures 6c and 6d report the results at 21 d. Figures 6a & 5c report Cl concentration measured by μXRF. Figures 6b & 6d report the Cl$^-$ concentration, predicted by the FE simulation described in [16], and the Cl concentration in Figures 6a & 6c along x = (1/4)W, (1/2)W. and (3/4)W. In Figures 6b & 6d, Cl concentration measurements, by μXRF, are plotted with dots and the shaded region indicates the measurement uncertainty estimated at a 95 % confidence level. FE simulation results are plotted with dashed or solid lines. Concentration is expressed in mol/m^3 of mortar.
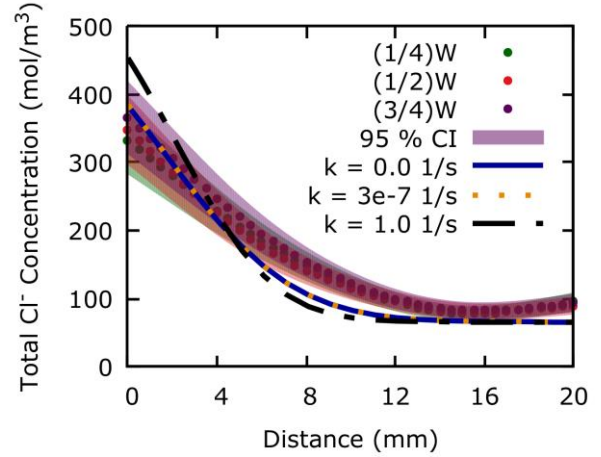
Cracked Mortar

Following the simulation procedures outlined in Jones et al., 2015 [13] and Bentz et al., 2013 [12], the chloride profile for two cracked domains are simulated by solving the mass balance equation described in [16] by the FE method. Figures 7 and 8 present a comparison between experimental measurements of chlorine concentration and FE simulation results for *w/c* = 0.4 and 0.5, respectively. The chlorine maps support results in [29], as the depth of penetration from the crack surface appears to be greater than that from the top, exposed surface. Jones et al. 2015 [13]

performed a series of FE simulations to model the chloride concentration around rectangular cracks. Following a similar procedure, in this study a region around the crack was defined to have a diffusivity greater than the bulk diffusivity by a factor DF. This assumption is based on the experimental results reported in [29], where chloride concentration measurements were made on the leachate of powdered mortar obtained by drilling to a known depth. This measurement technique may be used to estimate the diffusivity of the region sampled by the coring bit. With an approximate spatial resolution of 25 μm − it should be noted that the X-ray beam spot size is 50 μm, so in this study, spatial resolution indicates the approximate edge size of one pixel in the data set − the transport properties can be assessed at smaller length scales. With this enhanced measurement technique, Figures 7 and 8 indicate that DF is variable and is dependent on the crack geometry. The value of DF was estimated by varying its value in the FE simulation until the relative error between the FE results and chlorine measurements was minimized. Analysis of the damage zone diffusivity is given in [16] where DF is estimated from non-linear regression of Fick's 2nd Law along lines parallel to the x-axis. This study considers specimens with a maximum aggregate size of 2 mm. The value of DF depends on the cementitious material system of interest, including the maximum aggregate size. The method of determining DF described in this study, and in [16], is applicable to cementitious material systems with larger aggregates. The model detailed in this study addresses crack orientation by aligning the principal directions of the diffusivity tensor with the crack. These two factors improved convergence between experimental measurements and simulation results as shown in Figures 7b and 8b.

FE simulations predict the chloride concentrations near the top and bottom of the scanned area, but in the middle of the scanned area, the FE simulation results are greater than the measured chlorine concentration. The dips in the simulation results of Figures 7b and 8b are from regions where the model results are in the crack domain, which does not bind chlorides. The simulation results in Figure 8 agree well with the μXRF results, but do not appear to capture the behavior near the top surface. This is likely due to positional errors introduced into the model when converting the Si and Ca μXRF images into a format that can be accepted by the model. However, the behavior away from the top surface is in agreement with the chlorine measurements, and therefore, is a suitable approximation to the observed measurements.
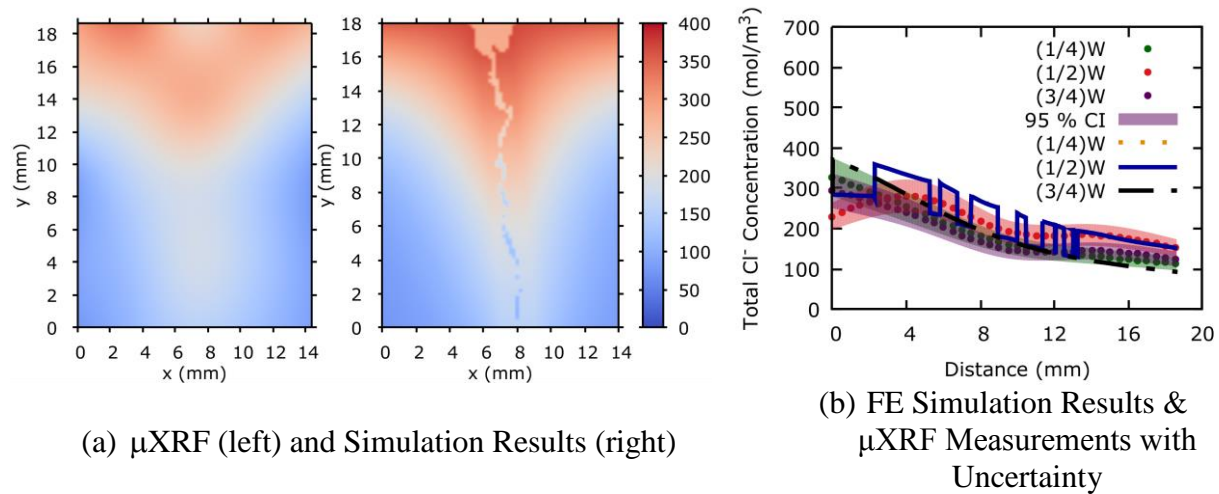

(a) μXRF (left) and Simulation Results (right)

(b) FE Simulation Results & μXRF Measurements with Uncertainty

Figure 7. Chlorine concentration in cracked specimen with w/c = 0.4 exposed to 1000 mol/m³ Cl⁻ for 14 d. (a) μXRF measurements and mass balance model solved by FE method with DF = 10 [16]. In (b), the Cl concentration, measured by μXRF, is plotted, with dots, from the

top surface along three parallel lines at x = (1/4)W, (1/2)W. and (3/4)W. The measurement uncertainty is estimated at a 95 % confidence level and is bounded by the shaded region around the measurement points. FE simulation results are plotted with solid or dashed lines.

(a) μXRF (left) and Simulation Results (right)

(b) FE Simulation Results & μXRF Measurements with Uncertainty

Figure 8. Chlorine concentration in cracked specimen with w/c = 0.5 exposed to 1000 mol/m^3 Cl$^-$ for 15 d. (a) μXRF measurements and mass balance model solved by FE method with DF = 20 [16]. In (b), the Cl concentration, measured by μXRF, is plotted, with dots, from the top surface along three parallel lines at x = (1/4)W, (1/2)W. and (3/4)W. The measurement uncertainty is estimated at a 95 % confidence level and is bounded by the shaded region around the measurement points. FE simulation results are plotted with solid or dashed lines.
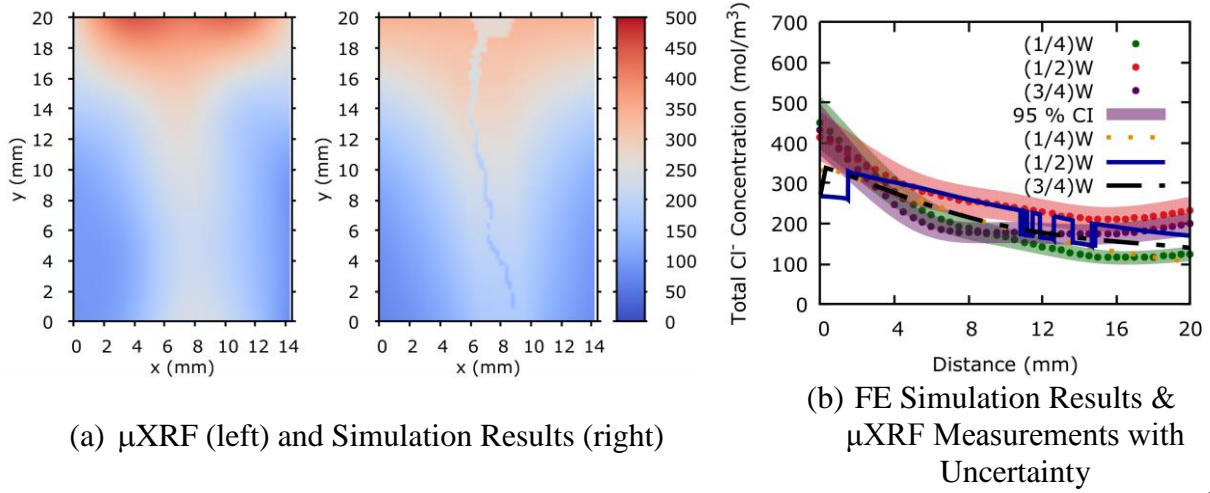
Crack-Filled Mortar

The results presented in Figure 9 report the chlorine concertation measured by μXRF and the chloride ion concentration predicted by the FE solution to the mass balance model for the case of an epoxy-filled crack. Because the epoxy crack filler overflowed the pre-crack notch and penetrated the top surface of the mortar, a rectangular region, on top of the pre-crack notice, was included in the epoxy domain as shown in Figure 4b. The width of the epoxy overflow was approximately 11 mm and is offset 0.5 mm to the right of the crack. Both the chlorine concentration measurements and the mass balance model capture the influence of the epoxy overflow, which is evident by the decrease in chlorine concentration in the region adjacent to the crack.

Figure 9b compares the chlorine measurements to the FE simulation. Outside the crack, the mass balance model is within the 95 % CI uncertainty range of the chlorine concentration measurements long the line located at x = (1/2)W. This is also the case for the results along the x = (1/4)W. The FE simulations do not fall within the 95 % CI for the chlorine measurements along the x = (3/4)W line. This discrepancy is likely due to the position of the epoxy overflow region in the model. Uncertainties in the dimensions of the overflowed area will influence model results; however, the global distribution of chlorides within the domain adjacent to the crack is captured by the model. When compared to the cracked case presented in Figure 7, the presence of the epoxy substantially reduces the chloride concentration at a given cover depth. Figure 9a does not show a measurable chlorine penetration between the mortar crack surface/crack filler interface, and the assumption of the damage zone returning to the diffusivity of the bulk mortar appears to be reasonable as the FE simulations are within the CI of the chlorine measurements.

Figure 10 reports chlorine concentration measurements and FE simulated results for the case of a methacrylate-filled crack. The width of the methacrylate overflow region was approximately 9 mm and was centered on the crack. The FE simulation predicts chloride ion concentrations that are within the 95 % CI of the chlorine measurement along the line located at x = (1/2)W. To the left and right of the crack, the mass balance model predicts the chloride ion concentrations is greater than the measured chlorine concentration. Microstructure variations due aggregate segregation or excesses bleed water may be a source of this discrepancy between the mass balance model and chlorine measurements. In addition, the placement and size of the overflow region will affect the FE simulation results. The uncertainty associated with these parameters may also be responsible for the observed difference between FE simulations and experimental measurements.

As with the epoxy crack filler, the methacrylate penetrates and seals the crack without transport of Cl^- between the crack filler and mortar. Neutron tomography studies in [14, 16] show that the methacrylate crack filler contained several voids. These voids do not appear detrimental to the ability of the crack filler to prevent chloride ion transport, as they are likely isolated and are not percolated throughout the mortar crack volume.
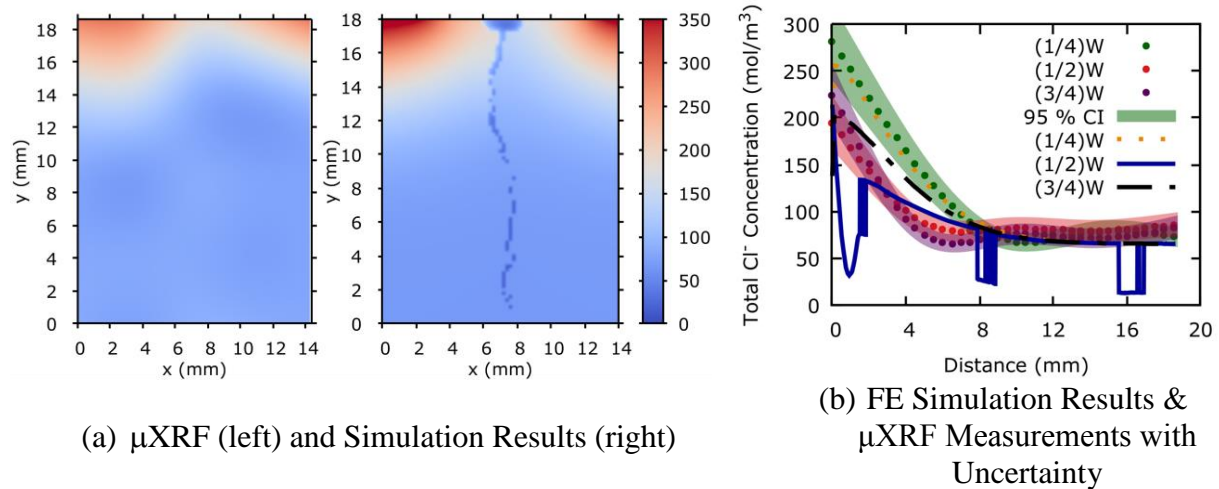

(a) μXRF (left) and Simulation Results (right)

(b) FE Simulation Results & μXRF Measurements with Uncertainty

Figure 9. Chlorine concentration in a cracked specimen repaired with an epoxy crack filler. Mortar w/c = 0.4 and exposed to 1000 mol/m^3 Cl^- for 14 d. (a) μXRF measurements and (b) mass balance model solved by FE method with DF = 1 [16]. In (b), the Cl concentration is plotted with dots along three parallel lines at x = (1/4)W, (1/2)W, and (3/4)W. The measurement uncertainty is estimated at a 95 % confidence level and is bounded by the shaded region around the measurement points. FE simulation results are plotted with solid or dashed lines.
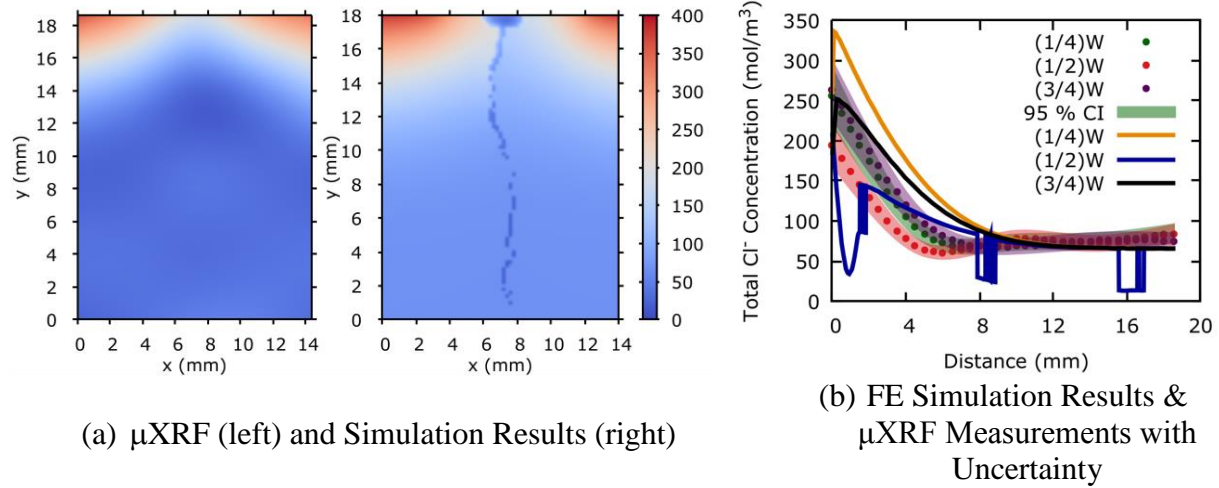
(a) μXRF (left) and Simulation Results (right)

(b) FE Simulation Results & μXRF Measurements with Uncertainty

Figure 10. Chlorine concentration in a cracked specimen repaired with a methacrylate crack filler. Mortar w/c = 0.4 and exposed to 1000 mol/m^3 Cl$^-$ for 14 d. (a) μXRF measurements and (b) mass balance model solved by FE method with DF = 1 [16]. In (b), the Cl concentration is plotted with dots along three parallel lines at x = (1/4)W, (1/2)W, and (3/4)W. The measurement uncertainty is estimated at a 95 % confidence level and is bounded by the shaded region around the measurement points. FE simulation results are plotted with solid lines.

Crack Filler Overflow

Confining the crack filler to the open space created by the formation of the crack is both cost and time prohibitive, for field applications, as the region around the crack would have to be isolated from the crack during the crack filling procedure. The presence of the crack filler overflow may have a beneficial effect on service life as it may prevent further chloride ingress. To study the influence of the crack filler overflow region, the chloride transport model was applied to the crack geometry in Figure 4b. The overflow region is located above the pre-crack notch and is assigned the transport properties of the crack filler. In this set of studies, an epoxy-based crack filler is assumed. The simulation is run to a time of 365 d, and the specimen is assumed to be submerged in a 1000 mol/m^3 chloride solution continuously throughout the simulation period. This simulation protocol is repeated for the same crack geometry with and without the overflow region.

Figure 11 reports the simulation results at times of 1 month, 3 months, 9 months, and 12 months. In Figures 11a through 11d, the left plot is the simulation case without the overflow region, and the right plot is the simulation case with the overflow region. Iso-concentration lines are plotted with their labels, and the units of concentration in this figure are mol/m^3. The domain plotted in Figure 11 corresponds to the scanned domain of Figure 9, which is a subset of the simulation domain pictured in Figure 4b.

Figures 11a through 11d shows that the effect of the crack filler overflow region is diminished as time increases. This is indicated by the convergence of the chloride concentration profiles in the domains with and without the overflow region. The plot to the right in Figure 11a shows the effect of the crack filler overflow, as it is apparent that the region below the pre-crack notch is at a lower concentration than that in the left side plot. The iso-concentration lines show a concentration gradient that is two-dimensional, and there is a flux of chloride ions penetrating under the overflow region. In Figure 11b, the iso-concentration lines highlight the effect of the overflow region at 9 and 12 months. In Figures 11c and 11d, respectively, the concentration

19

gradient around the overflow region is less pronounced. By 12 months, the left and right images resemble one another, and the magnitude of the iso-concentration lines is approximately the same at a given y-value. The apparent effectiveness of the crack filler overflow region is reduced as time increases, which is a result of the two-dimensional flux around the edges of the overflow regions. While not studied here, the size of the overflow region, or the distance it extends beyond the pre-crack notch, will likely affect the time required for the two simulation scenarios to converge.
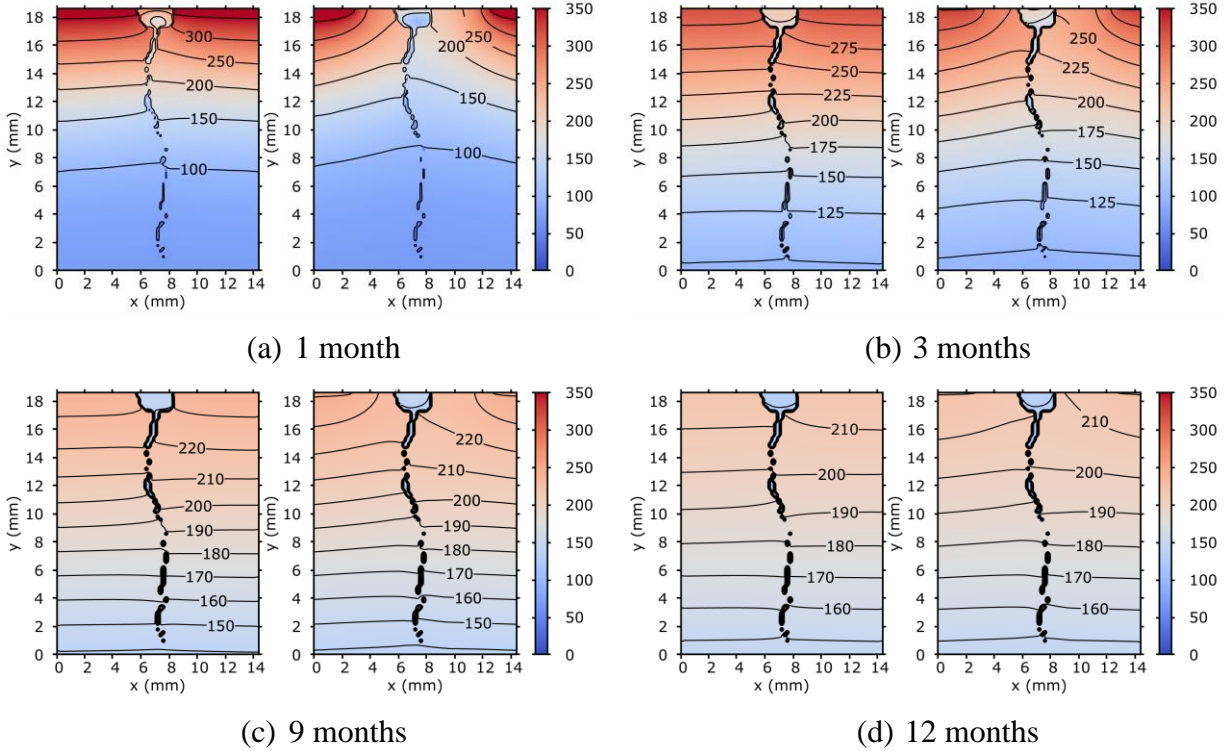

(a) 1 month

(b) 3 months

(c) 9 months

(d) 12 months

Figure 11. Cl^- concentration predicted by FE method solution to the mass balance model, described in [14], in epoxy-filled specimen without overflow region (left) and with overflow region (right) for (a) 1 month, (b) 3 months, (c) 9 months, and (d) 12 months exposure to a 1000 mol/m^3 Cl^- solution. By 6 months, the Cl^- concentration in the sample with the overflow region resembles the sample without it.

Crack Filler Penetration

The penetration of the epoxy crack filler into the mortar surrounding the crack is reported in Figure 12 and was estimated to be 0.37 mm with a standard deviation of 0.25 mm, while the penetration of the methacrylate crack filler was estimated to be 0.25 mm with a standard deviation of 0.18 mm. Both epoxy and methacrylate appear to show a measurable level of penetration into the mortar. The magnitude of the standard deviation relative to the measured penetration depth suggests that this penetration is not uniform along the crack. To improve upon this measurement, simultaneous X-ray and neutron tomography will be required. X-Ray tomography will detect aggregates, and, when added to the neutron tomography images, a better estimation of the empty crack width can be achieved. Decreasing the pixel resolution will sharpen the peaks of the crack filler and improve detection of the transition from cement paste to crack filler.

In [16], the surface tension of these crack fillers was measured using a Du Noüy Ring Tensiometer as a function of time after mixing. Results indicate that the epoxy crack filler reaches a hardened state at a time greater than 1.8 h after mixing while the methacrylate hardens within 20 min. The epoxy is able to penetrate farther into the mortar because it remains in a liquid state longer allowing for more time for penetration. This result suggests a balance between quick-setting epoxies and their viscosities must be maintained to ensure that the lower viscosity materials can take advantage of their viscosities to completely fill and penetrate cracks.
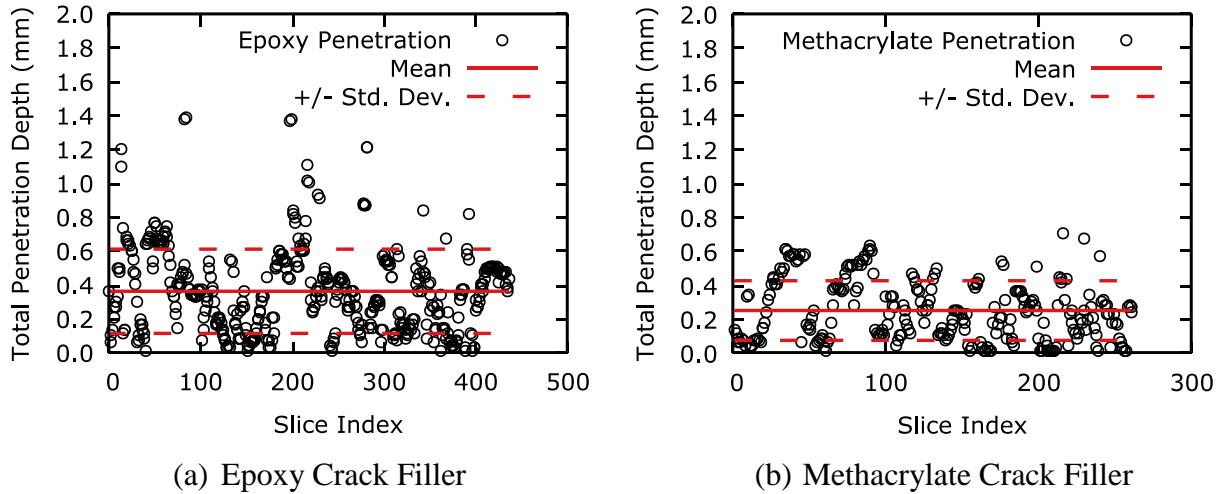

(a) Epoxy Crack Filler   (b) Methacrylate Crack Filler

Figure 12. Estimated crack filler penetration for (a) epoxy-filled crack and (b) methacrylate-filled crack. Penetration depth is total penetration into the mortar from each side of the crack.

Leaching of Chlorine from Crack Filler

Wavelength Dispersive X-ray Fluorescence measurements indicate that the epoxy crack filler contains approximately 4 % Cl. While the exact chemical formulation of the crack fillers is proprietary, the SDS provided by the manufacturer indicates the Cl is contained in the $C_{15}H_{16}O_2 \cdot C_3H_5ClO$ component. To determine if this Cl is bound in the epoxy or if it can be leached from the crack filler to the mortar, three samples of both epoxy and methacrylate were exposed to a solution of pH 13 composed of 48 mol/m^3 of NaOH and 55 mol/m^3 of KOH. Table 6 reports the chloride concentration in the storage solution at various time points for each sample. Measured values and uncertainties are derived from measurements made using a Cl$^-$ selective electrode as described in [16].

The measured chloride concentration, reported in Table 6, show that the Cl contained in the epoxy and methacrylate does not leach from the crack filler. The measured values are near zero when compared to the results obtained from the same measurement technique performed on de-ionized water. In addition, the lowest concentration level achieved in the calibration of the chloride selective electrode was 1.00E-05 mol/m^3. All measurements in Table 6 are 2 to 4 orders of magnitude lower, further indicating that the chloride concentration in the storage solution of the crack fillers is at or near zero.

Table 6. Chloride concentration in storage solution of epoxy and methacrylate specimens.

Sample ID	Mass (g)	EQBM Conc. (mol/m^3)	Time (d)	Measured Conc. (mol/m^3)	Meas. Uncert. (mol/m^3)
E1	5.45	161	3	2.55E-08	0.92E-08
			36	1.69E-08	0.64E-08
E2	8.02	238	3	8.28E-09	3.15E-09
			36	3.35E-09	1.37E-09
E3[1]	7.88	233	3	2.08E-08	7.34E-09
			36	4.26E-09	1.72E-09
M1	5.34	1	3	6.01E-08	1.99E-08
			36	2.76E-09	1.13E-09
M2	5.61	1	3	3.66E-08	1.24E-08
			36	2.35E-09	0.98E-09
M3[1]	5.54	1	3	4.68E-08	1.58E-08
			36	2.79E-09	1.17E-09
DI H$_2$O	--	--	3	3.37E-08	1.15E-08

[1]After 31 d, these samples were moved to a 40 °C environment.

Conclusion

Capturing the influence of a crack on the transport of chloride ions into concrete structures is necessary to produce service life models that represent the in-service conditions of reinforced concrete structures. Microbeam X-ray fluorescence measurements, calibrated to the mixture proportions of interest, provide quantitative chlorine concentration measurements that are used to represent chloride ion transport from a concentrated solution into the mortar. A GAM can interpolate the µXRF measurements to produce a smooth, two-dimensional profile of the chlorine concentration within the specimen while retaining the concentration gradient produced by the presence of the crack. These results are suitable for model validation.

A two-dimensional mass transport model that includes the geometry of a crack and includes the time-dependent behavior of the mortar diffusivity, chloride binding isotherm and chloride binding reaction rate produces a chloride concentration profile that is within the measurement uncertainty of the calibrated µXRF measurements. The model can be extended to the case of polymer-filled cracks and can produce a chloride concentration profile that agreements with µXRF measurements. Results indicate that polymer-based crack fillers are an effective means of reducing the ingress of chlorides into mortar specimens, as they seal both the crack and the surrounding damage zone. Extending the transport model to the case of an overflow region above the crack revealed that this region provides additional protection from chloride ingress. Over time, as measured in terms of the simulation, the concentration profiles of cracks with and without the

overflow region begin to converge to each other, indicating that the added benefit of the overflow region is temporary. The epoxy-based crack filler contained an elevated amount of chlorine, when compared to the methacrylate and mortar that does not contain chlorine, however, subjecting the epoxy to a pH 13 solution did not cause the chlorine to be released from the epoxy.

Acknowledgements

References

1) Neville, A., "Chloride Attack of Reinforced Concrete: An Overview," *Materials and Structures,* **28** (2), 63, 1995.
2) Darwin, D., Browning, J., and Lindquist, W.D., "Control of Cracking in Bridge Decks: Observations from the Field," *Cement, Concrete, and Aggregates*, **26** (2), 148-154, 2004.
3) Bentz, D.P., and Weiss, W.J., "Internal Curing: A 2010 State-of-the-Art Review," NISTIR **7765**, U.S. Department of Commerce, February 2011.
4) Harikrishnan, N., Ozyildirim, C., and Sprinkel, M.M., "Reducing Cracks in Concrete Bridge Decks Using Shrinkage Reducing Admixtures," Report FHWA/VTRC 16-R13, Virginia Transportation Research Council, Charlottesville, VA, March 2016, available at: http://www.virginiadot.org/vtrc/main/online_reports/pdf/16-r13.pdf .
5) Bentz, D.P., Stutzman, P.E., Sakulich, A., and Weiss, W.J., "Study of Early-Age Bridge Deck Cracking in Nevada and Wyoming," NISTIR **7841**, U.S. Department of Commerce, January 2012.
6) Lindquist, W.D., Darwin, D., Browning, J., and Miller, G.G., "Effect of Cracking on Chloride Content in Concrete Bridge Decks," *ACI Materials Journal*, **103** (6), 467-473, 2006.
7) Guide to Concrete Repair. Rep. no. 546R-16. ACI Committee 546 Repair of Concrete, American Concrete Institute. Farmington Hills: American Concrete Institute, n.d. Print. ISBN: 978-0-87031-933-4.
8) Code Requirements for Assessment, Repair, and Rehabilitation of Existing Concrete Structures and Commentary. Rep. no. 562-16. ACI Committee 562 Evaluation, Repair, and Rehabilitation of Concrete Buildings, American Concrete Institute. Farmington Hills: American Concrete Institute, n.d. Print. ISBN: 978-1-942727-90-3.
9) Birdsall, A.W., Guthrie, W.S., and Bentz, D.P., "Effects of Initial Surface Treatment Timing on Chloride Concentrations in Concrete Bridge Decks," *Transportation Research Record: Journal of the Transportation Research Board*, No. 2029, Design of Structures 2007, Transportation Research Board, National Research Council, Washington, D.C., 103-110, 2007.
10) Smith, K.L., and Romine, A.R., "Materials and Procedures for Sealing and Filling Cracks in Asphalt-Surfaced Pavements – Manual of Practice," Report No. FHWA-RD-99-147, Federal Highway Administration, 1999, 108 pp.

11) Lu, Y., Garboczi, E.J., Bentz, D.P., and Davis, J.M., "Modeling Chloride Transport in Cracked Concrete: A 3-D Image-Based Microstructure Simulation," *Proceedings of the 2012 COMSOL conference,* Boston, MA, 2012.

12) Bentz, D.P., Garboczi, E.J., Lu, Y., Martys, N., Sakulich, A.R., and Weiss, W.J., "Modeling of the Influence of Transverse Cracking on Chloride Penetration into Concrete," *Cement and Concrete Composites.* **38**, 65-47, 2013.

13) Jones, S.Z., Martys, N.S., Lu Y., and Bentz, D.P., "Simulation Studies of Methods to Delay Corrosion and Increase Service Life for Cracked Concrete Exposed to Chlorides," *Cement and Concrete Composites*, **58,** 59-69, 2015.

14) Jones, S.Z., Bentz, D.P., Snyder, K.A., Martys, N.S., Hussey, D.S., and Jacobson, D.L., "Service Life Modeling of Reinforced High Volume Fly Ash (HVFA) Concrete Structures Containing Cracks," Proceedings International Concrete Sustainability Conference, Miami, FL, 15 pp., May 2015.

15) Jones, S.Z., Davis, J.M., Molloy, J.L., Sieber, J.R., and Bentz, D.P., "Modeling and Measuring Chloride Ingress into Cracked Mortar," Sustainable Construction Materials and Technologies 4, Las Vegas, August 7-11, 2016, 10 pp.

16) Jones, S.Z., "Chloride Ion Penetration in Cracked Mortar with Crack Fillers: Experiments and Modeling," Ph.D. Thesis, University of Maryland Baltimore County, 2016.

17) ASTM Standards, Vol. 04.01, Cement, Lime, and Gypsum, ASTM International, West Conshohocken, PA 2016.

18) Park, J., C hen, Y.-M, Kukor, J.J., and Abriola, L.M. " Influence of Substrate Exposure History Biodegradation in porous medium." Journal of Contaminant Hydrology, **51**, 233-256, 2001.

19) Luping, T. and Nilsson, L.O.. "Chloride Binding Capacity and Binding Isotherms of OPC paste and mortars." Cement and Concrete Reseasrch, **27**, 971-978, 1997.

20) Barneyback Jr., R.S., and Diamond, S., "Expression and Analysis of Pore Fluids from Hardened Cement Pastes and Mortars," *Cement and Concrete Research*, **11** (2), 279-285, 1981.

21) Bentz, D.P., Feng, X., and Hooton, R.D., "Time-dependent Diffusivities: Possible Misinterpretations Due to Spatial Dependence," in *Testing and Modeling the Chloride Ingress into Concrete. Proceedings. 2nd International RILEM Workshop.* September 11-12, Paris, France, 225-233, 2000.

22) Vapnik, V.N., The Nature of Statistical Learning Theory, Springer, New York, 1995.

23) James, G., et al. An Introduction to Statistical Learning with Applications in R, Springer, New York, 2013.

24) Wood, S.N., Generalized Additive Models: An Introduction with R. CRC Press, New York, 2011.

25) Jacobson, D.L., Hussey, D.S., Baltic, E., Larock, J., Arif, M., Gaglirg, J., Owejain, J., and Trabold, T., "Neutron Radiography and Tomography Facilities at NIST to Analyze In-Situ PEM Fuel Cell Performance," Neutron Radiography, 50-57, 2008.

26) R Core Team (2016). R: A language and environment for statistical computing. R Foundation for Statistical Computing, Vienna, Austria. URL   https://www.R-project.org/.

27) Wood, S.N. (2011) Fast stable restricted maximum likelihood and marginal likelihood estimation of semiparametric generalized linear models. Journal of the Royal Statistical Society (B) 73(1):3-36.

28) Hans Werner Borchers (2016). pracma: Practical Numerical Math Functions. R package version 1.9.5. https://CRAN.R-project.org/package=pracma.

29) Şahmaran, M., and Yaman, İ. Ö., "Influence of Transverse Crack Width on Reinforcement Corrosion Initiation and Propagation in Mortar Beams," *Canadian Journal of Civil Engineering*, **35** (3), 236-245, 2008.

30) JCGM 101:2008; *Evaluation of Measurement Data – Supplement 1 to the "Guide to the expression of uncertainty in measurement" – Propagation of Distributions Using a Monte Carlo Method*; Joint Committee for Guides in Metrology (JCGM), 2008.

31) Carde, C., and Francois, R., "Effect of ITZ Leaching on Durability of Cement-Based Materials," *Cement and Concrete Research,* **27**(7), 971-978, 1997.

32) Jenkins, R., and De Vries, J.L., *Practical X-Ray Spectrometry*. New York: Springer-Verlag p. 118, 1975.